JGR Earth Surface

RESEARCH ARTICLE
10.1029/2023JF007065

Storm Impacts on Mineral Mass Accumulation Rates of Coastal Marshes

L. Cortese[1], X. Zhang[1], Marc Simard[2], and S. Fagherazzi[1]

[1]Department of Earth and Environment, Boston University, Boston, MA, USA, [2]Jet Propulsion Laboratory, California Institute of Technology, Pasadena, CA, USA

Abstract Coastal marsh survival may be compromised by sea-level rise, limited sediment supply, and subsidence. Storms represent a fundamental forcing for sediment accumulation in starving marshes because they resuspend bottom material in channels and tidal flats and transport it to the marsh surface. However, it is unrealistic to simulate at high resolution all storms that occurred in the past decades to obtain reliable sediment accumulation rates. Similarly, it is difficult to cover all possible combinations of water levels and wind conditions in fictional scenarios. Thus, we developed a new method that derives long-term deposition rates from short-term deposition generated by a finite number of storms. Twelve storms with different intensity and frequency were selected in Terrebonne Bay, Louisiana, USA and simulated with the 2D Delft3D-FLOW model coupled with the Simulating Waves Nearshore (SWAN) module. Storm impact was analyzed in terms of geomorphic work, namely the product of deposition and frequency. To derive the long-term inorganic mass accumulation rates, the new method generates every possible combination of the 12 chosen storms and uses a linear model to fit modeled inorganic deposition with measured inorganic mass accumulation rates. The linear model with the best fit (highest R^2) was used to derive a map of inorganic mass accumulation rates. Results show that a storm with 1.7 ± 1.6 years return period provides the largest geomorphic work, suggesting that the most impactful storms are those that balance intensity with frequency. Model results show higher accumulation rates in marshes facing open areas where waves can develop and resuspend sediments. This method has the advantage of considering only a few real scenarios and can be applied in any marsh-bay system.

Plain Language Summary To offset sea-level rise and sinking land, coastal marshes need to increase their elevation through sediment deposition. Thus, sediment availability, which controls the deposition, represents a vital parameter to evaluate the resilience of these delicate ecosystems. The Terrebonne basin (Louisiana, USA) is an example of a coastal area isolated from sediment sources that is rapidly losing land. Here, storms are a vital process because they can resuspend and transport significant volumes of sediment from the ocean and coastal areas to the marshes. However, quantifying their contribution is not trivial because of their intermittent and variable nature. In general, the more intense the storm, the lower its frequency. We simulated 12 storms and calculated the amount of sediment deposited by each of them. Then, we combined deposition with frequency and found that storms bringing the largest volume of sediments are not the most intense ones, but those that balance intensity with frequency. Using a combination of our simulations, we derived long-term deposition rates (i.e., how much sediment is deposited on a yearly basis), which allow us to identify areas where marshes are resilient. This study shows that storms are fundamental for the survival of coastal marshes with limited sediment supply.

Key Points:

- A 2D depth averaged numerical model is coupled with a wave model to simulate sediment deposition by storms in Terrebonne Bay (Louisiana, USA)
- In Terrebonne Bay, storms with a return time of about 2 years have the highest geomorphological impact
- We use a novel method that combines simulations of storms of different intensity and frequency to derive inorganic mass accumulation rates

Supporting Information:

Supporting Information may be found in the online version of this article.

Correspondence to:

L. Cortese,
lucacort@bu.edu

Citation:

Cortese, L., Zhang, X., Simard, M., & Fagherazzi, S. (2024). Storm impacts on mineral mass accumulation rates of coastal marshes. *Journal of Geophysical Research: Earth Surface*, *129*, e2023JF007065. https://doi.org/10.1029/2023JF007065

Received 8 JAN 2023
Accepted 13 FEB 2024

Author Contributions:

Conceptualization: L. Cortese, S. Fagherazzi
Data curation: L. Cortese
Formal analysis: L. Cortese
Funding acquisition: Marc Simard, S. Fagherazzi
Investigation: L. Cortese, S. Fagherazzi
Methodology: L. Cortese, S. Fagherazzi
Project administration: Marc Simard, S. Fagherazzi
Resources: S. Fagherazzi
Software: L. Cortese, X. Zhang
Supervision: S. Fagherazzi
Validation: L. Cortese
Visualization: L. Cortese
Writing – original draft: L. Cortese
Writing – review & editing: Marc Simard, S. Fagherazzi

1. Introduction

The value of coastal marshes has been widely recognized. Carbon and nutrient uptake, refuge for unique wildlife, and storm surge buffering are among the many ecosystem services that they provide (Barbier et al., 2011, 2013; Chmura et al., 2003; Costanza et al., 1997; Hopkinson et al., 2012; Shaw & Fredine, 1971; Wamsley et al., 2010). However, the vulnerability of coastal marshes is increasing because of higher sea levels (Church & White, 2006; Sweet et al., 2022), decreased riverine sediment supply (Syvitski et al., 2005; Syvitski & Kettner, 2011), subsidence (Syvitski et al., 2009), and salinity intrusion (White & Kaplan, 2017; Wilson et al., 2018).

Marsh resilience is linked to its ability to maintain elevation against rising waters, which is achieved through a combination of inorganic sediment deposition and burial of organic matter. For the inorganic component, storms represent a fundamental driver of sediment supply (Ma et al., 2014; Mariotti & Carr, 2014; Mitchell et al., 2017).

The importance of storms has been observed for different tidal regimes. For example, storm-related deposition has been shown to be orders of magnitude higher compared to the deposition generated during tidal cycles in both microtidal and mesotidal marshes (Turner et al., 2006; Yang et al., 2003). Storms also alter intertidal flat morphology in macrotidal marshes, and therefore sediment fluxes to the marsh (De Vet et al., 2020).

During storms, the combination of enhanced sediment resuspension by wind waves and marsh inundation augment deposition over the marsh platform (Cahoon, 2006; Castagno et al., 2018; Tognin et al., 2021; Walters & Kirwan, 2016). However, storms also have a negative effect on coastal marshes. Storm generated waves can cause marsh edge erosion (Leonardi et al., 2016; Leonardi & Fagherazzi, 2014, 2015; Marani et al., 2011; Priestas et al., 2015) and trigger the loss of low salinity marshes (Howes et al., 2010). Sediments that are brought over the marsh during a storm can originate from rivers or the bottom of nearby bays, channels, and mudflats. In addition, during storms, marshes themselves can act as a source of material (Pannozzo et al., 2023). In this case, the lateral erosion generated by waves impacting marsh edges provides additional material to the system (Hopkinson et al., 2018). This mechanism can be a non-secondary contribution to sediment deposition on marshes (Luk et al., 2021) at the expense of total marsh area.

Deriving deposition rates from storms is not trivial because these events are intermittent (Chen et al., 2021; Zhong et al., 2014) and are characterized by different magnitudes and return periods. It is not realistic to simulate all the storms occurring during long-term accumulation measurements at high temporal resolution, since they can span decades. Moreover, data necessary for modeling (e.g., water level, wind speed) are seldom available for such long periods.

In a storm, wind speed and direction, water level, and wave height vary in time, making it difficult to analyze the parameter space of these variables and run simulations covering all possible scenarios. Therefore, our goal is to use a limited set of real storms to produce a deposition pattern similar in terms of spatial variability to long-term mass accumulation rates. In this parsimonious approach, we use storms that cover the possible range of surges and wind conditions of the study area. We then determine which linear combination of the storms better predicts long-term inorganic mass accumulation rates. The storms represent a vector of independent events that we assume represent all the forcing of the system. As such, they are chosen during periods when extensive hydrodynamic measurements are available, and do not have to overlap the sediment accumulation measurements.

We set our analysis on the Louisiana coast along the northern Gulf of Mexico. This area includes around 40% of the total United States marshes (Penland et al., 1990) and represents a hot spot of marsh loss (Couvillion et al., 2017) with nearly 5,000 km^2 of marshland converted to open water in recent decades. A relative sea-level rise rate of 13 ± 9 mm/yr and a diminished sediment supply have been indicated as key factors for marsh deterioration (Day & Templet, 1989; Törnqvist et al., 2020; Yu et al., 2012). For instance, the proliferation of dams along the Mississippi River has reduced the suspended sediment load from 400 to 500 MT/year to 205 MT/yr (Blum & Roberts, 2009) and a sediment deficit of 9.34 ± 23.5 MT/year indicates a lack of material to sustain the current marshes (Sanks et al., 2020).

We focused our analysis on the inactive Terrebonne basin (Louisiana, USA). Here, the microtidal regime makes tidal currents less relevant for resuspension and transport of sediment over the marsh platform due to the short hydroperiod (Reed, 1989). Wang et al. (1993) found that marsh sedimentation in Terrebonne Bay is largely driven by strong winds. Therefore, only storms have the ability to remobilize and transport substantial volumes of sediment into the marsh platform. Consequently, the role of episodic storms and related surges needs to be addressed to quantify the long-term sediment deposition in the region.

This study shows that, in order to quantify the geomorphological effect of a storm, both magnitude and return period (i.e., frequency) must be accounted for. The proposed method can be implemented in any setting where storms represent a fundamental driver for sediment deposition on marshland and provide a general framework to account for storm impact on inorganic mass accumulation rates.

2. Methods

2.1. Study Area

The Terrebonne basin is located along the Louisiana coast between the Barataria and Atchafalaya basins (Figure 1). Tides are diurnal, with an average range of 40 cm (Georgiou et al., 2005). The western portion of the

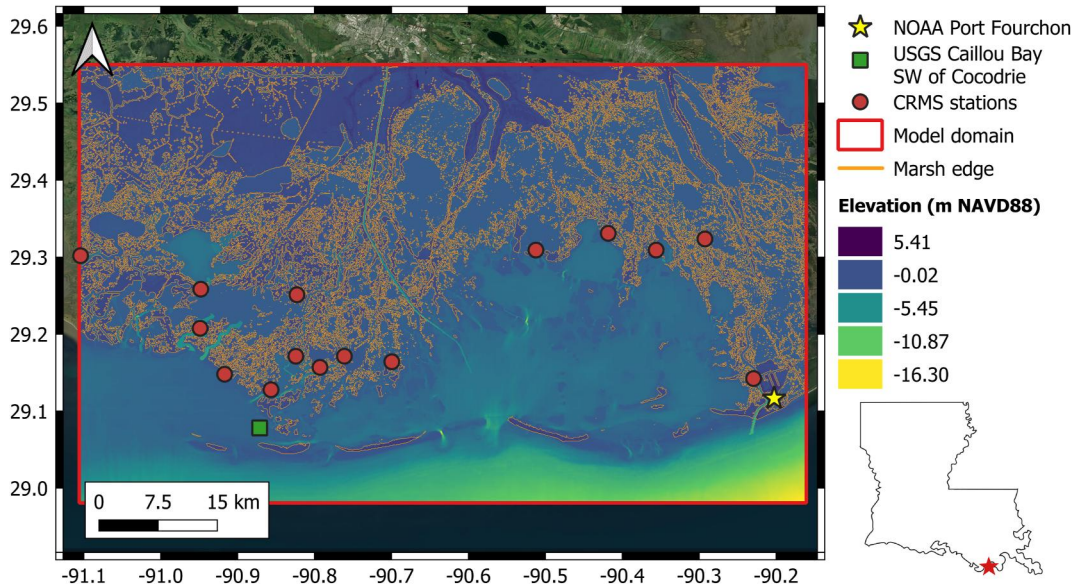

Figure 1. Terrebonne Bay, Louisiana, USA. The red rectangle outlines the domain of the numerical model and the red dots are the CRMS stations used for model validation. The USGS and NOAA stations are also indicated. The orange contour line delineates the edge of the marsh. The red star on the bottom right inset indicates the location of Terrebonne Bay in Louisiana.

bay has a slightly larger range compared to the eastern area close to Grande Isle (Hiatt et al., 2019). The entire coastal Louisiana is a hotspot for relative sea-level rise with rates in the range of 8–10 mm/yr (Sweet et al., 2022). Subsidence rates are variable across the bay and range between 3 and 8 mm/yr in the southern part and 3–5 mm/yr in the northern part (Byrnes et al., 2023). After the diversion of a Mississippi river distributary in 1903 (LBSE, 1904), the bay has no significant riverine sediment input supplying the adjacent marshes (Twilley et al., 2016). However, minor freshwater inputs are still present and control the salinity gradients between the coastal salt marshes and the inland freshwater marshes (Twilley et al., 2019). In turn, salinity gradients affect vegetation distribution with *Spartina alterniflora* dominating the saline marshes and *Spartina patens* dominating brackish areas (Sasser et al., 2014).

2.2. Storm Surges Selection

We computed each storm surge by subtracting the astronomical tidal signal from the measured water levels, both of which were provided by the National Oceanic and Atmospheric Administration (NOAA) station 8762075 located in Port Fourchon in the south-eastern portion of the Terrebonne basin. We assigned a 10 m/s wind speed and a 0.3 m residual water level as thresholds to identify a significant storm surge. These two thresholds allowed us to isolate tropical storms and depressions typically occurring during the hurricane season (01 June–30 November) and winter cold fronts. We also considered two surges below the 0.3 m threshold in order to account for small events, with water elevations close to the astronomical signal. Overall, we selected a total of 12 events covering different ranges of surge magnitude (Figure 2 and Table 1). All storms hit Terrebonne Bay between April 2019 and August 2021, apart from one event in 2008. The maximum surge and wind speed varied from 0.09 to 1.15 m and from 11 to 25.44 m/s respectively. To account for major events, we simulated Hurricane Zeta on 29 October 2020, which made landfall in Louisiana near Cocodrie as Category 3, and Hurricane Ike on 12 September 2008. The latter made landfall in Galveston (Texas); however, its passage generated a significant surge along the Louisiana coast.

The magnitude of a storm can be described in terms of surge, namely, the higher the surge, the stronger and more intense the storm. Another parameter used to characterize a storm is its return period. This parameter is defined as the average time between two events with same magnitude. High values indicate low frequency and large storm surge. To retrieve the return period, we used time series of water levels at the NOAA station in Port Fourchon. As a proxy for storm surge, we extracted the maximum water-level

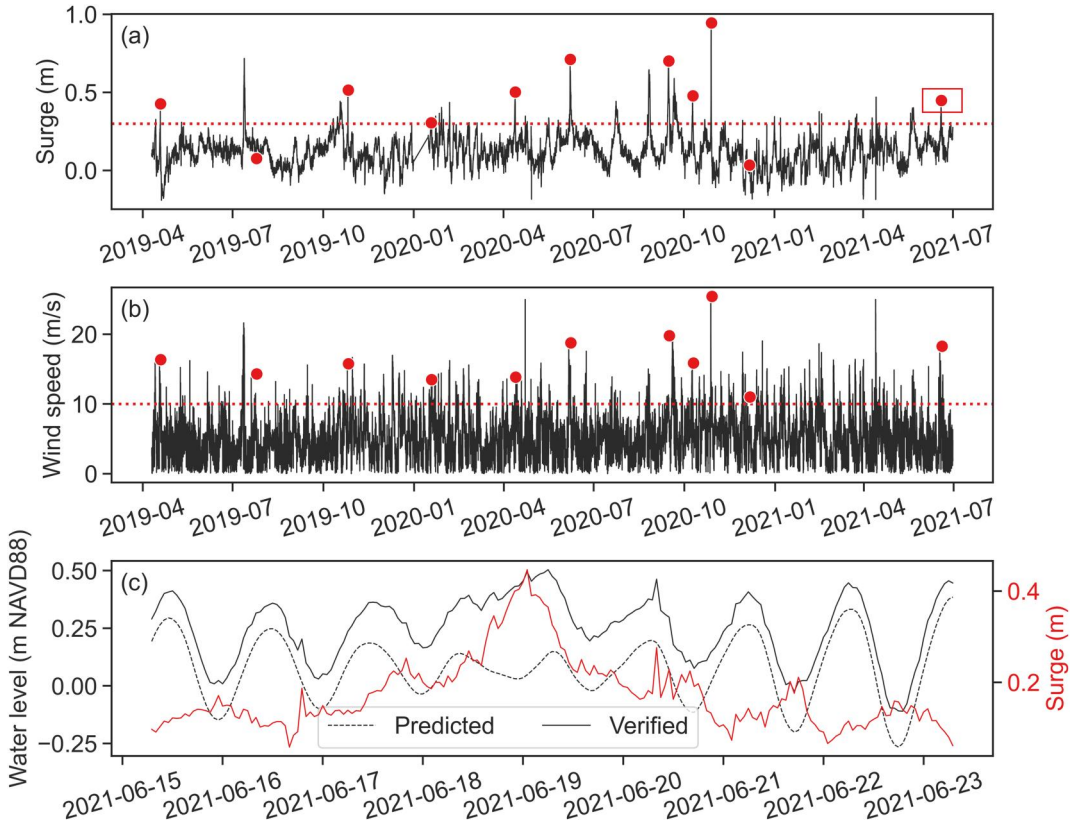

Figure 2. (a) Surge timeseries with the selected storms (red dots). The dashed red line indicates the 0.3 m threshold. The surge on 12 September 2008 is omitted for better visualization. (b) Wind speed timeseries with the selected storms. The dashed red line indicates the 10 m/s threshold. (c) Example of the storm surge in June 2021 (red rectangle in (a)). Note that predicted and verified in the legend refer to the water level.

value in each year (from July 2003 to November 2022), sorted them from smallest to largest, and computed a logarithmic fitting against the return period (Figure 3a). Then, we used the log equation to infer the return period of the 12 selected storms (Figure 3b).

Table 1
Date and Time of Surge Maximum, Maximum Water Level, Maximum Wind Speed, and Return Period for the 12 Selected Storm Surges

Storm ID	Storm date and time (dd-mm-yyyy hh:mm)	Max surge (m on NAVD88)	Max wind speed (m/s)	Return period (years)
Storm1	12-09-2008 08:00	1.15	21.90	13.42
Storm2	19-04-2019 00:00	0.41	16.36	1.69
Storm3	25-07-2019 16:00	0.15	14.31	0.82
Storm4	26-10-2019 10:00	0.52	15.78	2.3
Storm5	18-01-2020 18:00	0.32	13.50	1.52
Storm6	13-04-2020 01:00	0.5	13.86	2.17
Storm7	07-06-2020 20:00	0.7	18.78	3.79
Storm8	15-09-2020 17:00	0.71	19.80	3.90
Storm9	09-10-2020 19:00	0.48	15.87	2.05
Storm10	29-10-2020 00:00	0.95	25.44	7.50
Storm11	08-12-2020 16:00	0.09	11.00	0.68
Storm12	19-06-2021 07:00	0.45	18.28	1.89

Note. Time is expressed in US Central Time Zone.

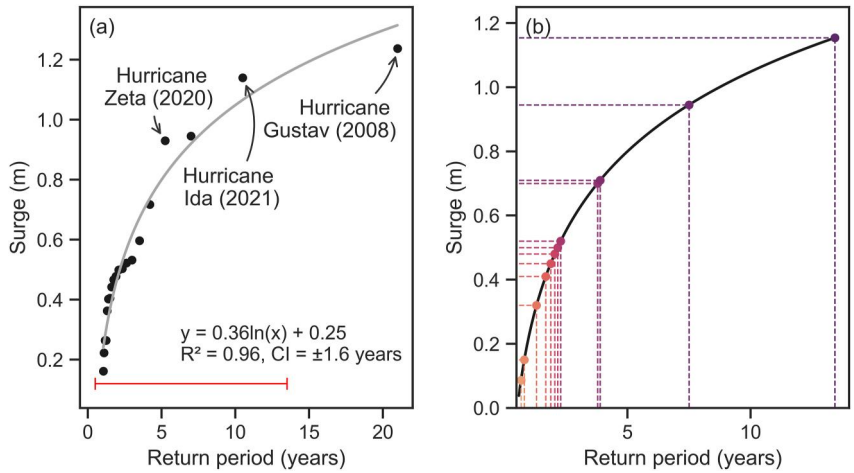

Figure 3. (a) Relationship between maximum surge by year and return period derived from the NOAA station in Port Fourchon (ID: 8762075). Data started from 2003. Log equation, R^2, and confidence interval are indicated at the bottom right. The surges generated by a few major events are indicated. The red bar in the lower left corner indicates the range of return periods explored in the simulations. (b) Detail of the relationship between surge and return period for the storms simulated in this study.

2.3. Models Set Up and Validation

For each storm, we developed a sediment transport model using the 2D depth-averaged Delft3D-FLOW module (Lesser et al., 2004) fully coupled with SWAN (Simulating Waves Nearshore, e.g., Booij et al., 1999; Holthuijsen et al., 1993; McLoughlin et al., 2015; Ris et al., 1999). In each simulation, we included 4 days before and after the surge peak (Figure 2b), so we were able to account for sediment removal immediately after the passage of the storm. Major storms can resuspend and transport large fluxes of sediments during the flood phase of a surge. However, it has been shown that the subsequent ebb phase might export a comparable volume of sediment (Fagherazzi & Priestas, 2010). The same research shows that moderate storms do not trigger the fast ebb flows responsible for sediment export and yield a positive net sediment input. For each model, we changed boundary conditions, wind speed, and wind direction without modifying the other parameters such as bottom friction, initial bathymetry, and sediment properties. The domain (Figure 1) covers the coastal area of the Terrebonne basin and consists of 1,139 × 686 cells with a 90 × 90 m resolution. Elevation data are referred to NAVD88 and available from NOAA (Love et al., 2010). Boundary conditions were imposed as water levels offshore the barrier island in the Gulf of Mexico. Water levels were taken from the United States Geological Survey (USGS) station 073813498 located near Pelican Lake in Caillou Bay (see Figure 1), as this station is close to the center of the domain. Only for the 12 September 2008 storm (Hurricane Ike), we used water levels recorded at the NOAA gauge at Port Fourchon. We calibrated the models by adjusting the water levels at the boundary (Abbott & Cunge, 1975; Cunge, 2003; Mariotti et al., 2010; Wiberg et al., 2015). The signal was delayed, and the amplitude was modified to reproduce the correct water levels at the USGS station. Wind speed and direction data were taken from the same station and applied homogeneously on the entire domain with hourly time resolution. Bottom friction was applied by imposing the Manning coefficient (Table 2), whose values are based on the USGS Louisiana Gap Analysis Project (LA-GAP) classification of vegetation cover (see Table 2, Hartley et al., 2000).

We considered two sediment types at the bottom of the bay: sand and mud. For each simulation, initial conditions were derived from the usSEABED database (Williams et al., 2006), which provides the fraction of mud and sand in several coastal locations. Overall, the bottom of the bay is mainly composed of mud, whereas sand is found along the barrier island system. For both fractions, sediment parameters are based on Liu et al. (2018) (Table 3).

Table 2
Manning Coefficients Used in the Model to Compute Bottom Friction

Marsh type	Water	Saline	Brackish	Intermediate	Fresh
Manning coefficient	0.02	0.035	0.045	0.05	0.055

The hydrodynamic models were validated by comparing the water levels with measurements recorded at 11 stations within the Coastwide Reference Monitoring System (CRMS). We selected stations in channels with a width of at least 270 m (3 mesh elements) (see Figure 1). Model performance was evaluated using three parameters: Nash-Sutcliffe Model Efficiency (NSME), Percentage Bias (PBIAS) and Root Mean Square Error (RMSE) (Allen

Table 3
Parameters Used for Sand and Mud Fractions in the Sediment Transport Model

Parameter	Density (kg/m^3)	D_{50} (mm)	Settling velocity (mm/s)	Critical shear stress for erosion (N/m^2)
Mud	1,600	–	0.25	0.1/1.0
Sand	2650	0.14	–	–

Note. If no value is specified, the corresponding parameter was not used in the formulation. For the critical shear stress for erosion, the smaller value was set in the channels and bay bottoms, while the larger value was used on the marsh surface.

et al., 2007). For additional validation, we ran the model from 25 March 2021 to 18 April 2021 and compared modeled water discharge with ADCP measurements collected during the Delta-X campaign (Christensen et al., 2022) and from 9 March 2012 to 25 March 2012 to compare modeled significant wave height with field measurements (Parker, 2014). The location of ADCP transects and wave gauge is indicated in Figure S1 in Supporting Information S1. Furthermore, since Mariotti et al. (2018) measured wind spatial variability in the area, we compared wind data between the USGS station selected for this study and the weather station located in Terrebonne Bay and maintained by the Louisiana Universities Marine Consortium (LUMCON). To address the effect of different wind timeseries on sediment deposition, we also ran a simulation of one storm using wind data from LUMCON. The location of the LUMCON station is reported in Figure S4 in Supporting Information S1.

2.4. Derivation of the Inorganic Mass Accumulation Rates

We considered a total of 37 CRMS sites (Table S1 in Supporting Information S1) where deposition is regularly measured using feldspar marker horizons in different plots. In this technique, a layer of at least 5 mm white feldspar clay is deposited on the marsh surface. Then, once or twice a year, the thickness of the newly deposited material is measured from the feldspar layer to the marsh surface. Measurements were taken from three cores at each plot. Cores were collected at each sampling site using a 10.2 cm inside-diameter core tube sharpened at the end and a PVC coring handle for insertion to a depth of about 30 cm. The collection started between 2006 and 2009. Despite the presence of gaps, values are collected twice per year until 2020 and once per year after 2020. We extracted and averaged deposition rates for each plot at each site. Given that the oldest plots are 10 years old, we considered only plots with a record of at least 8 years. In addition to deposition, soil bulk density (BD) and average percentage of organic matter (OM) were measured every 4 cm until a 24 cm depth on two dates: during plot establishment and in 2018. We averaged the values from the two dates to obtain a mean BD and OM. BD is measured from samples dry weight (oven dry at 60°C for 48 hr), while OM is measured with the loss-of-ignition technique (550°C for 2 hr) using the relationship (Folse et al., 2018):

$$\mathrm{OM} = \mathrm{Wt}\, B_{60} - \mathrm{Wt}\, A_{550} \,/\mathrm{Wt}\, B_{60} \quad (1)$$

where Wt B_{60} is the weight of the soil sample dried at 60°C and Wt A_{550} is the weight of the soil sample after ashing at 550°C. We refer to Wang et al. (2017) for more details on soil sample analysis.

The separation of mineral and organic mass accumulation rates was performed following Neubauer (2008). First, the organic bulk density (BD_O) was calculated as the product between BD and the OM fraction, so that the mineral bulk density (BD_I) was computed as the product between BD and (1-OM). Then, the inorganic mass accumulation rates (IMAR) were computed as the product between the average deposition from the feldspar marker horizon and BD_I. IMAR values for the stations included in the study are reported in Table S1 in Supporting Information S1.

2.5. Geomorphological Impact of Storms

In this study, we always refer to the sediment deposited by the storms as inorganic sediment, opposed to the organic material that is the result of local plant productivity. In particular, we use the term inorganic mass deposition (IMD, measured in g cm^{-2}) to indicate the amount of sediment deposition computed by the model. Consequently, to indicate long-term rates of deposition, we use the term inorganic mass accumulation rates (IMAR, measured in g cm^{-2} yr^{-1}).

The impact of each storm on the marsh was evaluated in a two-fold process. First, we directly related the total inorganic deposition to the maximum surge during each storm to observe the morphological impact on the event scale. Then, we computed the geomorphic work (*sensu* Wolman & Miller, 1960) by calculating the product of the total modeled deposition and the frequency of each event.

2.6. Linear Combination of Storms

First, we analyzed the deposition in each storm. Since there are no measurements of mineral deposition for each storm, to evaluate the goodness of the modeled deposition, we used the long-term inorganic mass accumulation rates derived from deposition measurements at each CRMS site. The comparison is carried out as a linear regression between the modeled inorganic mass deposition and the measured inorganic mass accumulation rates to capture the long-term spatial gradients in mineral deposition rates. Despite the comparison involves two different quantities measured on different time scales, this procedure can provide an indication of the goodness of the depositional pattern provided by the models.

Then, we extracted every possible combination of the 12 surges using m elements without repetition C(12, m), where $m = 2,\ldots,12$ is the number of surges considered for a generic combination. For each combination, we computed the total inorganic mass deposition (IMD) in each CRMS site by summing the modeled inorganic mass deposition of each surge (imd). For instance, when $m = 3$ the total IMD for one combination can be generally written as

$$\mathrm{IMD} = w_i \cdot \mathrm{imd}_i + w_j \cdot \mathrm{imd}_j + w_k \cdot \mathrm{imd}_k, i, j, k = 1, \ldots, 12 \;\&\; i \neq j \neq k \tag{2}$$

The term w is a weighting coefficient based on the return period and allows to give more weight to surges with high frequency. Given a combination of m surges, the generic coefficients can be written as

$$w_p = f_p / \sum_{p=1}^{m} f_p \tag{3}$$

where f_p is the frequency of the p-th surge and it is defined as the inverse of the return period (i.e., 1/yr). We also note that $\sum_{p=1}^{m} w_p = 1$. An explicit example of IMD derivation is reported in the Supporting Information S1. For each combination, we compared the total IMD to the inorganic mass accumulation rates to obtain a linear model that reads

$$\mathrm{IMAR} = x_1 \cdot \mathrm{IMD} + x_0 \tag{4}$$

where x_0 and x_1 are the intercept and slope respectively. We selected the linear model that provided the best fit (i.e., highest R^2) with measurements in 16 of the 37 selected CRMS sites (Table S1 in Supporting Information S1) and applied it across the Terrebonne domain to derive a map of inorganic mass accumulation rates. Finally, we validated the model by comparing its results to measured IMAR in other CRMS stations not used in the model derivation (Table S1 in Supporting Information S1).

3. Results

3.1. Hydrodynamic and Sediment Transport Models Validation

The comparison between the simulated and measured water levels indicates that all 12 models reproduced the storm surges with satisfactory performance (Figure 4).

Given the high NSME (>0.65) and low PBIAS (<±10) the performance level for all models can be categorized as excellent (Allen et al., 2007). We also observed a negative PBIAS in all cases, with an average underestimation of 1.6%. The comparison between measured and modeled water discharge (Figure S2 in Supporting Information S1) showed that the model was able to reproduce the water flow in five different cross sections with an RMSE of 56.756 m^3/s despite one case of large underestimation. In addition, the simulation of March 2012 showed that the model can reproduce the significant wave height (Figure S3 in Supporting Information S1) with a RMSE of 0.082 m. Finally, wind data from the USGS station were comparable to those from the LUMCON station (Figure S4 in Supporting Information S1) with an RMSE varying between 1.92 and 3.46 m/s.

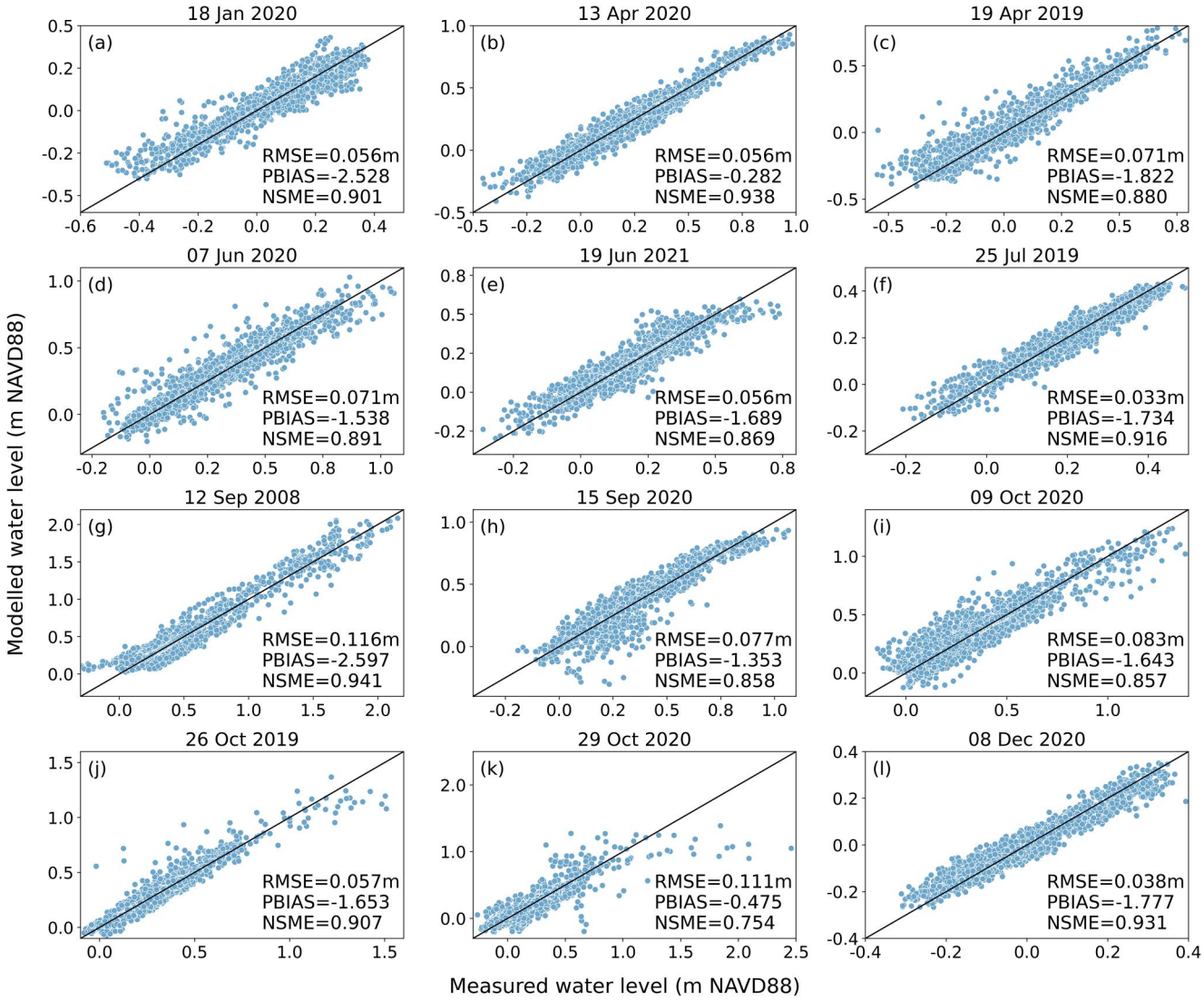

Figure 4. Comparison between modeled and measured water levels. In each subplot, all 11 CRMS stations are included. Each station has 192 points, thus a total of 2112 points in each subplot. The corresponding storm date is written on top of the subplot. In each subplot, the model performance indices RMSE, PBIAS and NSME are indicated.

The comparison of the modeled deposition with the inorganic mass accumulation rates allowed us to evaluate whether the models capture the deposition pattern (Figure 5). Overall, 8 out of 12 simulations showed a significant correlation. We found no correlation in the three simulations with the lowest surges and Storm 12 (Figures 5a, 5e, 5f, and 5l), indicating that if storms are not included, many areas of the marsh remain unflooded and do not receive sediment. We also ran a simulation of Storm 2 using the LUMCON wind data, since it was the case with the highest RMSE (see Figure S4c in Supporting Information S1) between the USGS and LUMCON wind speed timeseries. The simulation returned 2.12 MMT (Million Metric Tons) of deposited sediment. Since the simulation with USGS wind data returned 2.03 MMT, we concluded that the different source of wind data does not make a significant impact on the deposited sediment.

3.2. Sediment Deposition Analysis

To integrate event frequency into the inorganic deposition rates, we computed the geomorphic work. This parameter is the product between deposition and event frequency. By considering the surge level as independent variable, we interpolated both deposition and frequency with log equations (Figure 6a). The geomorphic work is

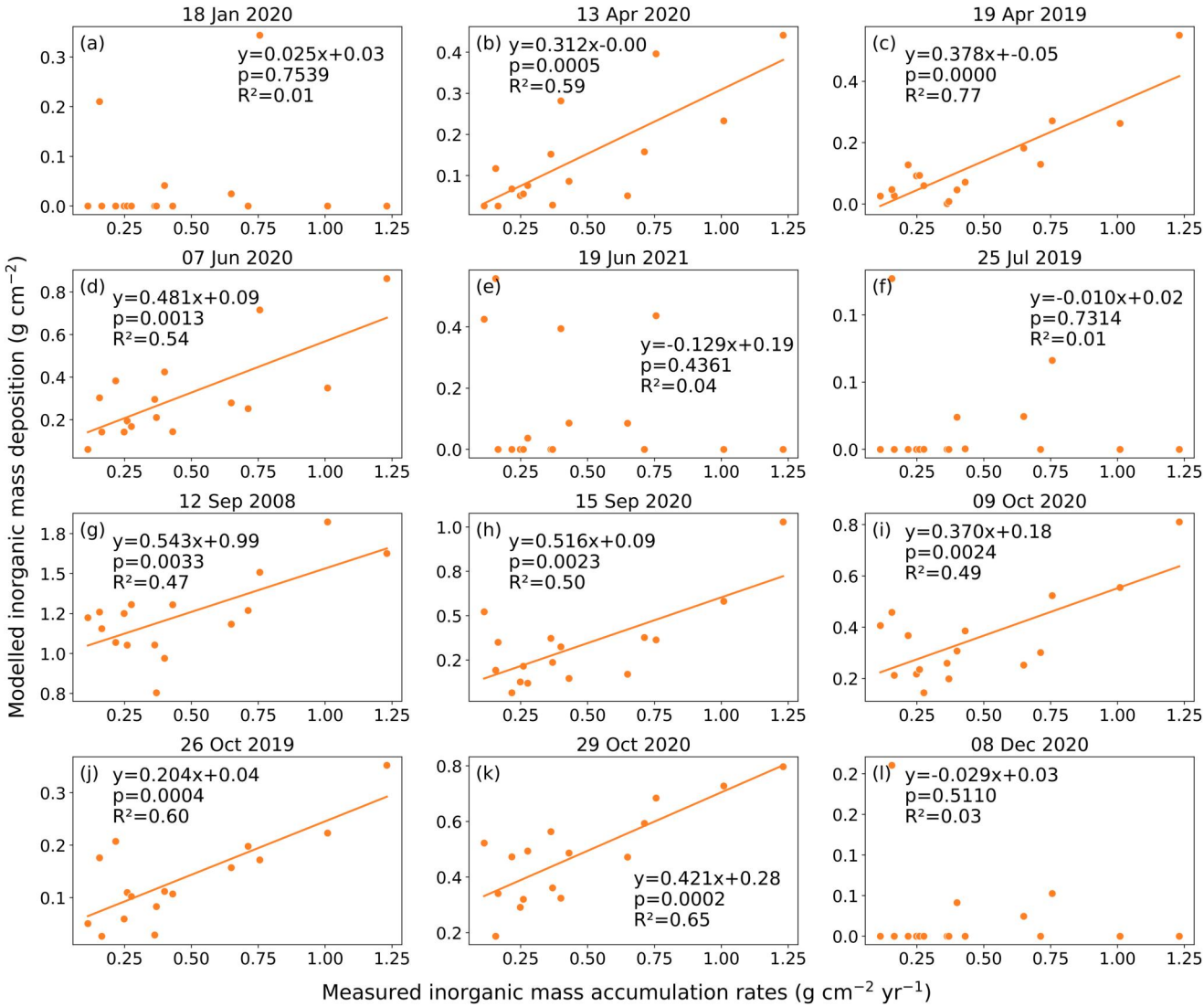

Figure 5. Comparison between measured long-term inorganic mass accumulation rates and the modeled deposition for all 12 models. In each subplot, the storm date is indicated on the top. Regression lines are drawn only in cases of statistical significance (p-value < 0.05).

displayed with the solid black line in Figure 6b. The result showed a relationship with a maximum value that does not correspond to the highest surge (Figure 6b). We found that the surge of 19 April 2019 (0.41 m above NAVD88, green dot in Figure 6b) represents the highest geomorphic work. The lowest geomorphic work corresponds to storms with low magnitude and high return period or storms with high magnitude and low return period. Moreover, when we only considered the simulations that provided a significant correlation between measured accumulation and modeled deposition, a power law provided the best fit.

3.3. Linear Combinations of Storm Surges and Inorganic Mass Accumulation Rates

The combination of Storms 2, 6, and 8 provided the best fitting with the long-term inorganic accumulation mass rates measured at the CRMS sites (Figure 7a, with an R^2 of 0.79). The weights (computed with Equation 3) were 0.45, 0.35, and 0.2 for the first, second, and third storms, respectively. The linear equation reads:

$$\mathrm{IMAR} = 1.44 \cdot \mathrm{IMD} + 0.12 \quad (5)$$

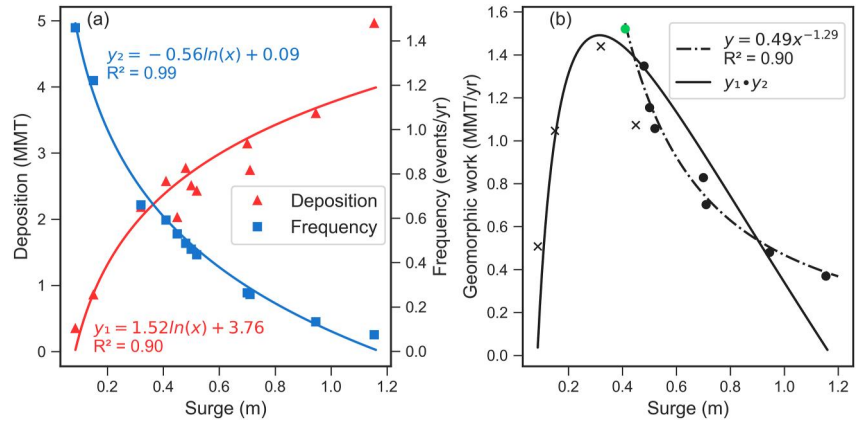

Figure 6. (a) Relationship between surge and deposition (in red) and surge and frequency (in blue). (b) Relationship between the geomorphic work of each event and surge level. The solid dots indicate surges for which we found a significant relationship in Figure 5, whereas the crosses indicate surges without significant relationship. The solid line represents the geomorphic work expressed as the product of the two equations in panel (6a), while the dash-dotted line represents the power law fitting the solid black points. The green dot highlights the simulation on 19 April 2019, which has the highest geomorphic work.

where *IMAR* (g cm^{-2} yr^{-1}) is the inorganic mass accumulation rate and *IMD* (g cm^{-2}) is the combined inorganic mass deposition from the storm surge models. We also explored how different combinations tend to represent the measured IMAR (Figure 7b). The two highest values of R^2 were found for a combination of 2 and 3 storms; as we increased the number of storms, the regressions were increasingly less representative with a lower R^2. After applying the linear model for every point in the domain (Figure 8), we validated the model by comparing its results to inorganic mass deposition rates measured in other CRMS stations not included in the analysis. The validation (Figure 7c) provided an RMSE of 0.19 g cm^{-2} yr^{-1}. We also observed that the model is both underestimating and overestimating the measured inorganic mass accumulation rate, in particular around 0.2 and 0.6 g cm^{-2} yr^{-1}.

From Figure 8, we observe that the inorganic mass accumulation rates range from 0.12 to 1 g cm^{-2} yr^{-1} in the model domain. The highest rates of accumulation are found along the bay and areas bordering open water, while moving inland and to high elevations, the inorganic accumulation rates drop drastically.

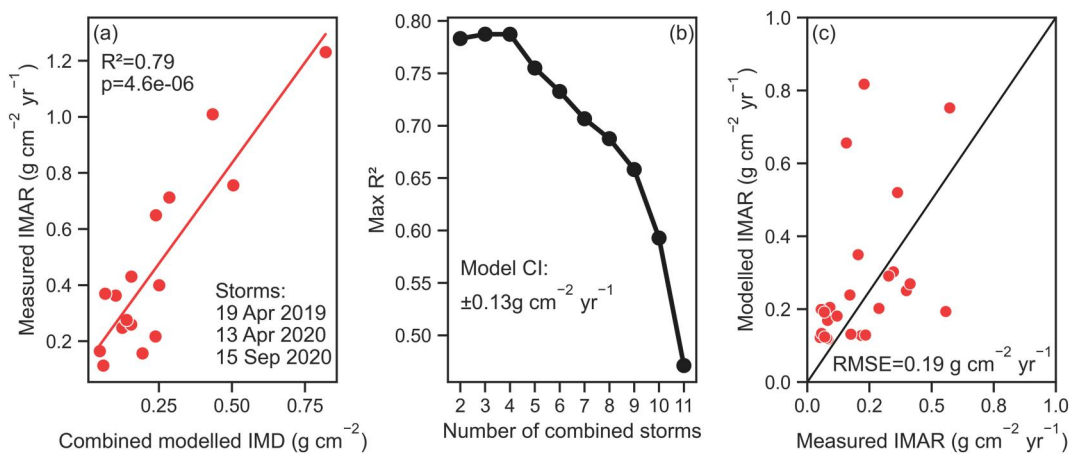

Figure 7. Results from the combination of storm surges. (a) Linear regression between the combined modeled inorganic deposition and the measured inorganic mass accumulation rates. On the lower right, the three selected storm surges are indicated. (b) Maximum R^2 for each category of combined storms and model confidence interval. (c) Validation of the linear model applied to other CRMS stations.

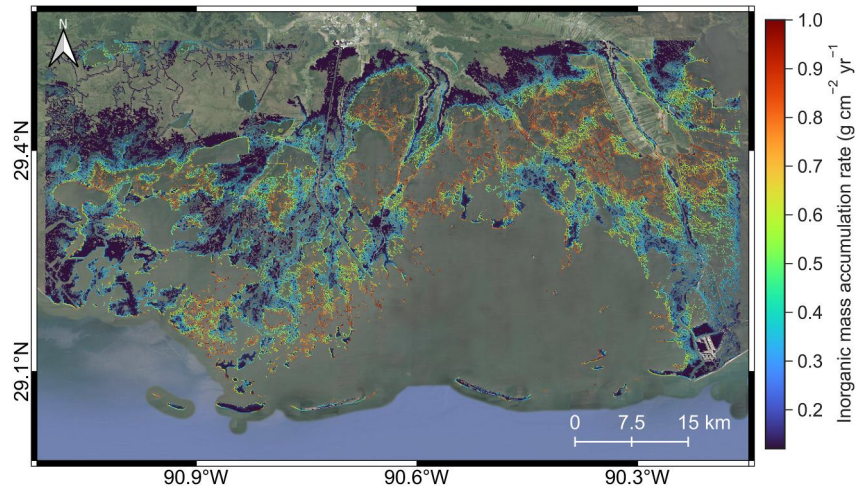

Figure 8. Modeled inorganic mass accumulation rates in Terrebonne. The map is obtained by applying Equation 5 to the entire domain, which includes the combination of three storms (19 June 2019, 13 April 2020, and 15 September 2020).

4. Discussion

4.1. Geomorphological Impact of Storms on Inorganic Accumulation Rates

Modeling sediment deposition is the key to determine the fate of coastal marshes affected by sea-level rise and land subsidence (Fagherazzi et al., 2020). Spatial maps of inorganic accumulation can indicate more resilient or vulnerable areas. However, in marshes where sediment transport is controlled by intermittent events, this task becomes problematic as there is no regular pattern and running numerical simulations at high temporal resolution for decades is not possible. In this study, we addressed the issue by simulating a prescribed set of storm surges and combining them to produce a realistic forecast that accounts for both magnitude and frequency of storms. This approach differs from the more traditional methodology of running a limited number of fictional scenarios in which a set of parameters such as surge, relative sea level, and wind speed are changed (e.g., Mariotti et al., 2010; Pannozzo et al., 2021). Note that our simulations are short, lasting 8 days, while the inorganic mass accumulation rates are measured in years. Therefore, our proposed method implicitly assumes that our simulations capture the general physics of storm surges and their long-term effects on depositional rates.

To fully reproduce storms, it is fundamental to include both the surge and waves (Zhu & Wiberg, 2022). Under stormy conditions, wind waves enhance bottom shear stresses and entrain more sediment in the water column (Carniello et al., 2005; Green & Coco, 2014). Higher water levels generate longer hydroperiods and consequently a higher suspended sediment volume over the marsh (Wiberg et al., 2020). A surge further contributes to sediment entrainment due to enhanced currents. Waves can also influence the maximum surge and the inundation distance depending on storm characteristics, especially during weak events (Wu et al., 2018).

We found that the deposition is correlated with the surge maximum elevation (Figure 6a), indicating that at the event scale, higher surge events contribute more in terms of deposition.

The Louisiana coast is well-known to be affected by tropical cyclones (Georgiou et al., 2005). Previous research has highlighted the beneficial role of these extreme events for salt marsh accretion. Cahoon et al. (1995) analyzed the impact of Hurricane Andrew in the Terrebonne, Barataria, and Pontchartrain basins and found high contributions to short-term deposition (1–3 orders of magnitude higher than in the pre-storm conditions). Turner et al. (2006) estimated a contribution of 131×10^6 metric tons along the entire Louisiana Coast from Hurricanes Katrina and Rita in 2005. Liu et al. (2018) computed 27 metric tons of sediment imported from Hurricane Gustav in 2008 between the Terrebonne and Barataria basins (10.8 and 16.2 tons respectively). However, the above-mentioned events have high return periods, and therefore low temporal frequency. For instance, the logarithmic model in Figure 3a shows that despite having the highest short-term impact in terms of surge, Hurricane Gustav has a return time of 21 years. Tweel and Turner (2014) analyzed the impact of major and moderate hurricanes in Louisiana and found that frequent moderate storms account for 78% of the long-term sedimentation rates.

Thus, storm frequency is the key to understand marsh accretion and resilience to sea-level rise. Previous modeling studies have highlighted that storm frequency is almost two times more efficient in increasing marsh deposition compared to storm magnitude, and therefore frequent storms enhance marsh adaptability to future sea-level rise scenarios (Schuerch et al., 2013). By computing the product between deposition and frequency (i.e., geomorphic work), we were able to evaluate the impact of each event on a yearly basis. From Figure 6b, we conclude that storms with the highest impact in terms of deposition have a return period of 1.7 years. Therefore, in terms of long-term mineral deposition, the most impactful events balance magnitude with frequency.

Results in Figure 7 suggest that a combination of three storms can provide reliable estimates of long-term accumulation rates in Terrebonne Bay. The optimal combination includes Storm 2 (the surge with the highest geomorphic work), Storm 6 (the surge with the third highest geomorphic work and a return time of 2.2 years), and Storm 8 (the second most intense storm after the hurricanes with a return time of 4 years). Interestingly, this combination included two storms with high geomorphic work, which combined contributed for 80% of the total inorganic deposition, while the remaining 20% was attributed to a storm with a very high surge. The combination suggests that moderate and frequent storms are more responsible for the long-term inorganic deposition, whereas intense storms, despite providing a non-negligible contribution, have lower long-term impact.

Wind direction represents an important factor that was not considered in the selection of the storm surges. If the wind direction is aligned with the largest fetch, the potential to develop higher waves increases leading to more sediment resuspension at the bottom (Fagherazzi & Wiberg, 2009). Moreover, water levels increase along the wind direction. In Terrebonne Bay, southerly winds augment water levels and promote marsh flooding and consequent transport of sediments over the marsh. Around 39% of all wind data used in the simulations have northerly direction, while 61% have a southerly direction (Figure S5 in Supporting Information S1), displaying good coverage. The highest wind speeds occur for southerly directions, indicating that the selected events present favorable conditions for the transport of sediments in the marsh. Interestingly, two of the three selected storms (see Figure 7a) are extra-tropical storms (i.e., winter storms) and show the typical pattern observed during cold fronts (see an example in Figure S6 in Supporting Information S1). The pre-frontal phase characterized by southerly winds (Figure S6c in Supporting Information S1) anticipates the frontal passage where the wind direction quickly shifts to northerly winds in the post-frontal phase (Figure S6c in Supporting Information S1) (Moeller et al., 1993). Previous research has shown that winter storms in coastal Louisiana and in particular cold fronts control the wave fields (Cao et al., 2020; Guo et al., 2020), water fluxes (Feng & Li, 2010), and sediment exchange (Dingler & Reiss, 1990; Perez et al., 2000; Roberts et al., 1989). Reed (1989), using sediment deposition measurements in Terrebonne Bay, suggested that cold fronts represent an ideal setting for sediment deposition. The southerly winds promote the mobilization of the sediment in the coastal bays and enhance water level in the marsh (Figure S6a in Supporting Information S1), while the subsequent northerly winds lower the water levels (Figure S6a in Supporting Information S1) and favor the drainage of the marsh and the consolidation of the newly deposited sediment. It is worth noting that a later study by Murray et al. (1993) in Terrebonne Bay showed that some cold fronts resulted in a net export of sediment from the marsh system.

Validation of the linear model suggests an overall overestimation of inorganic mass accumulation rates (Figure 7c). The two notable overestimation cases occurred for stations 978 and 3,296, where we modeled 0.66 g cm^{-2} yr^{-1} instead of 0.16 g cm^{-2} yr^{-1}, and 0.82 g cm^{-2} yr^{-1} instead of 0.23 g cm^{-2} yr^{-1}respectively. These errors could be related to the elevation of the marsh. Marsh elevation was derived from Light Detection and Ranging (LiDAR), which has been shown to have a positive bias due to the inability to penetrate marsh vegetation (Ewald, 2013; Rogers et al., 2018). Even small topographic inaccuracies can lead to wrong flooding patterns (Zhang et al., 2022), which can lead to wrong deposition values. A lower elevation can enhance flooding and allow more sediment to deposit. We also observed a case of underestimation at site 338, where we modeled 0.19 g cm^{-2} yr^{-1} instead of 0.58 g cm^{-2} yr^{-1}. At this site, inorganic mass accumulation rates are among the highest because of the proximity to the open bay. As in overestimation cases, elevation can be a reason for the underestimated values, as in high areas flooding is more limited.

The linear model allowed us to compute inorganic mass accumulation rates at every point of the Terrebonne Bay domain (Figure 8). The spatial distribution showed higher rates in the proximity of large channels and open water areas (i.e., the source of sediments) because they have enough fetch to develop wind waves, while sheltered areas located inland have lower rates due to the absence of riverine sediment load and low inorganic transport from weak tidal currents (Cortese & Fagherazzi, 2022). This result is consistent with observations in Terrebonne from

Reed (1989), which found higher deposition in sites closer to Terrebonne Bay. The spatial pattern is also consistent with Tweel and Turner (2012), which examined the deposition after four tropical cyclones and found decreasing deposition with distance from the coast. Field measurements by Smith et al. (2021) in coastal Mississippi showed that most of the sediment was deposited within 10 m from the shoreline. A similar pattern was found in European marshes with meso-macrotidal semidiurnal regimes (Reed et al., 1999; Temmerman et al., 2003).

4.2. Storms as a Degrading Factor

This study analyzed the beneficial role of storms in coastal marshes that lack riverine sediment supply. However, storms have been shown to negatively impact marshes through lateral erosion (Leonardi et al., 2018). Storms can thus have a two-fold effect on marshes; they promote accretion and vertical resilience while degrading the marsh laterally (Cortese & Fagherazzi, 2022). Sediment deposited on the marsh platform can also be remobilized during storms, but this is very uncommon since the dense vegetation reduces currents and attenuates waves. In all our simulations, storms produced net deposition with limited remobilization. The remobilization of sediment deposited on the marsh surface, if present, can introduce uncertainty in the relationship between storm deposits and long-term accumulation rates.

Hurricanes deposit large amounts of inorganic sediments that can cause soil compaction with a net loss of marsh surface elevation (Cahoon, 2006). Storms can also have a negative impact on wetland vegetation. Rodgers et al. (2009) showed that the combination of hurricane Katrina and a subsequent drought prevented vegetation recovery for more than 1 year, probably triggered by the increased salinity. Most importantly, the combination of currents and waves shear stresses can remove vegetation through root scalping and promote later erosion (Priestas et al., 2015). Low salinity marshes are more vulnerable due to the shallow rooting and lower soil shear stress resistance (Howes et al., 2010).

Wave power has generally been related to marsh lateral erosion (e.g., Houttuijn Bloemendaal et al., 2023; Leonardi et al., 2016; McLoughlin et al., 2015). Waves can deepen tidal flats facing marsh edges and consequently enhance wave energy (Fagherazzi et al., 2006). However, the impact of waves on marsh edges can be highly variable due to the heterogeneity of soil resistance and biological processes (Leonardi et al., 2018). During moderate storm conditions, marshes are more vulnerable because their boundaries are exposed to wave action (Fagherazzi, 2014). In this case, waves trigger undercutting and the collapse of the marshes margin (Marani et al., 2011). However, during extreme events, when water levels are higher than the marsh platform, waves pose a lesser threat to the margins (Fagherazzi, 2014). In Louisiana, marsh edge erosion is highly dependent on the direction the marsh faces. South-facing marshes experience high water levels and limited erosion, whereas north-facing marshes experience low water levels and have higher probability of undercutting (Valentine & Mariotti, 2019). In Terrebonne Bay, the role of waves on marsh retreat was extensively presented by Everett et al. (2019). Their results clearly show the impact of both wind and swell waves on marsh lateral erosion. In particular, they found high retreating rates correlated with swell waves propagating through gaps between barrier islands. As the barrier islands in Terrebonne are slowly deteriorating, wave erosion might increase in the future.

4.3. Implications for Marshes Survival

Previous measurements of sediment concentration and deposition highlighted that tidal currents do not transport significant quantities of sediment in Terrebonne Bay (e.g., Reed, 1989; Wang et al., 1993). On a larger scale, storm-driven sediment transport has been proposed to be the dominant component of inorganic deposition in Louisiana (Tweel & Turner, 2012), and widespread land loss not related to a lack of inorganic sediment supply but to a diminished organic accumulation (Turner et al., 2007).

Our method leverages on storm surges to provide a spatially distributed estimate of the present inorganic accumulation rates. However, we do not suggest that sediment delivered by storms can balance sea-level rise and subsidence. Jensen et al. (2022) showed that the Terrebonne basin lost about 472 km^2 of land. Total accretion rates (organic and inorganic) measured by CRMS indicate that the Terrebonne basin has a deficit of sediment and cannot sustain current rates of relative sea-level rise (Jankowski et al., 2017; Sanks et al., 2020). Thus, relying on the contribution of storms might not be sustainable in the future (Burkett et al., 2007; Törnqvist et al., 2007). For instance, Smith et al. (2015) showed that despite storm-driven sediment is relevant for vertical accretion, the major contribution to long-term accumulation is given by river diversions. An important factor in marsh survival

is the source of the sediment. Deposited sediment can originate from the redistribution of the previously eroded marsh soil (Hopkinson et al., 2018) and not from the inland transport of offshore material.

4.4. Limitations and Broader Impacts of Our Approach

The primary hypothesis of our method is that the contribution to inorganic deposition in Terrebonne is dominated by storms. Regular tides can also contribute to inorganic mass deposition. For instance, Smith et al. (2021) estimated an accumulation rate of 0.0008 g cm^{-2} $tide^{-1}$ in the Grand Bay estuary in southeast coastal Mississippi, which has tidal ranges similar to Terrebonne. Our simulations with very small storm surges indicate that tides do not produce significant geomorphic work and that their deposition pattern does not match long-term accumulation rates. Therefore, storms are the chief geomorphic agent in Terrebonne Bay.

In our analysis, we did not examine the relative contribution of mud and sand in each event. Due to the ability to resuspend coarser grains, sediment deposition after intense storms can produce soil textures different from those produced during weaker storms or non-storm events (Nyman et al., 1995).

The small deposition rates found in the internal areas of the domain can be related to the distance from the sediment source, as observed earlier, but also to a limitation of the model. Many areas within the Terrebonne region are fed by channels with cross sections ranging in the tens of meters or smaller. Given the coarse mesh resolution of the model (90 m), solving water levels and fluxes in internal areas is difficult. Future developments could rely on either unstructured mesh or subgrid-scale modeling to better solve narrow channels. It is also worth noting that in the validation of water discharges (Figure S2 in Supporting Information S1), the model underestimates values by 18% when the outlier point is discarded. The underestimation of the discharge can reduce the transport of sediment inside the marsh, possibly underestimating sediment concentration and deposition.

Despite its limitations, our model can provide maps of inorganic accumulation rates. These maps might also indicate areas of high organic accumulation; in fact, a high inorganic sediment load produces favorable environmental conditions to sustain bioproductivity because it provides nutrients to the plant sustainment and reduces the concentration of toxic substances (such as free sulfite) by improving soil aeration (Mendelssohn & Kuhn, 2003).

Storm frequency and intensity might vary in the future because of climate change and sea-level rise (Karl et al., 2009; Knutson et al., 2010). As extreme events become more frequent, the most impactful storms could be different with respect to those considered in this analysis. As a result, the combination of storms used in the regression could change and a different set of storms might be needed to better represent the measurements. In this context, the method presented here is well-suited to account for this variability and can be applied to any marsh-bay system independent of tidal range.

5. Conclusions

We quantified the contribution of storms to inorganic mass accumulation rates on salt marsh platforms by investigating the combined effect of storm magnitude and intensity. At the event scale, intense storms provided the highest inorganic deposition. However, more frequent storms generated larger geomorphic work and long-term contribution to the deposition, suggesting that geomorphologically impactful events balance magnitude with frequency. We proposed a new empirical approach that takes in account a selection of storms, combines them based on magnitude and frequency, and provides a linear relationship to derive inorganic mass accumulation rates. This linear model yields a parsimonious set of simulations that captures the spatial distribution of the inorganic mass accumulation rates consistent with field measurements. The proposed method has the advantage of being highly flexible and applicable to any marsh-bay system.

Conflict of Interest

The authors declare no conflicts of interest relevant to this study.

Data Availability Statement

The inorganic mass accumulation rates map is available via the ORNL DAAC Delta-X data portal at https://doi.org/10.3334/ORNLDAAC/2301 (Cortese & Fagherazzi, 2023). Data supporting the modeling are publicly

available. CRMS stations water levels, accretion, and soil properties data are available via the CPRA website (https://cims.coastal.louisiana.gov/monitoring-data/). Bathymetric data used for the models are available via the National Center for Environmental Information website (https://www.ncei.noaa.gov/metadata/geoportal/rest/metadata/item/gov.noaa.ngdc.mgg.dem:1521/html) (Love et al., 2010). Astronomical and measured water-level data used to derive storm surges and return periods from the NOAA gauge 8762075 at Port Fourchon are available via the Tides & Currents website (https://tidesandcurrents.noaa.gov/stationhome.html?id=8762075). The mud and sand fraction used to define the bottom of the bay and channels in the models are available via the USGS usSEABED website (https://www.usgs.gov/programs/cmhrp/science/usseabed) (Williams et al., 2006). Water-level data used as boundary conditions for the model, wind speed, and wind direction from the USGS gauge 073813498 are available via the USGS website (https://waterdata.usgs.gov/monitoring-location/073813498/#parameterCode=00065&period=P7D). Wind speed and direction data from the LUMCON Terrebonne Bay weather station used to evaluate the effect of wind variability on the results were made available upon request from LUMCON and can be seen via the website (http://weatherstations.lumcon.edu/). Water discharge data used to validate the model are available via the ORNL DAAC Delta-X data portal (https://daac.ornl.gov/cgi-bin/dataset_lister.pl?p=41) (Christensen et al., 2022). Wave significant height data used to validate the wave model were taken from Parker (2014).

Acknowledgments

The authors are grateful for the comments provided by Q. Jim Chen and two other anonymous reviewers, which greatly improved the presentation and impact of this study. This research was funded by the NASA Delta-X project (the Science Mission Directorate's Earth Science Division through the Earth Venture Suborbital-3 Program NNH17ZDA001N-EVS3). L.C. was supported by the Future Investigators in NASA Earth and Space Science and Technology (FINNEST) award number 80NSSC21K1612. S.F. was also supported by the Virginia Coast Reserve Long-Term Ecological Research Program (National Science Foundation DEB-1832221) and the Plum Island Ecosystems Long-Term Ecological Research Program (National Science Foundation OCE-2224608). Part of this work was performed at the Jet Propulsion Laboratory, California Institute of Technology, under contract with the National Aeronautics and Space Administration (NASA).

References

Abbott, M. B., & Cunge, J. A. (1975). Two-dimensional modeling of tidal deltas and estuaries. In *Unsteady flow in open channels* (Vol. 2, pp. 763–812).

Allen, J. I., Somerfield, P. J., & Gilbert, F. J. (2007). Quantifying uncertainty in high-resolution coupled hydrodynamic-ecosystem models. *Journal of Marine Systems*, *64*(1–4), 3–14. https://doi.org/10.1016/j.jmarsys.2006.02.010

Barbier, E. B., Georgiou, I. Y., Enchelmeyer, B., & Reed, D. J. (2013). The value of wetlands in protecting southeast Louisiana from hurricane storm surges. *PLoS One*, *8*(3), e58715. https://doi.org/10.1371/journal.pone.0058715

Barbier, E. B., Hacker, S. D., Kennedy, C., Koch, E. W., Stier, A. C., & Silliman, B. R. (2011). The value of estuarine and coastal ecosystem services. *Ecological Monographs*, *81*(2), 169–193. https://doi.org/10.1890/10-1510.1

Blum, M. D., & Roberts, H. H. (2009). Drowning of the Mississippi Delta due to insufficient sediment supply and global sea-level rise. *Nature Geoscience*, *2*(7), 488–491. https://doi.org/10.1038/ngeo553

Booij, N. R. R. C., Ris, R. C., & Holthuijsen, L. H. (1999). A third-generation wave model for coastal regions: 1. Model description and validation. *Journal of Geophysical Research*, *104*(C4), 7649–7666. https://doi.org/10.1029/98jc02622

Burkett, V., Groat, C. G., & Reed, D. (2007). Hurricanes not the key to a sustainable coast. *Science*, *315*(5817), 1366–1368. https://doi.org/10.1126/science.315.5817.1366

Byrnes, M. R., Hollis, R. J., Khalil, S. M., Britsch, L. D., Berlinghoff, J. L., Raynie, R., & Haywood, E. (2023). Recent subsidence trends in Terrebonne Basin, Louisiana. In *Coastal sediments 2023: The Proceedings of the Coastal Sediments 2023* (pp. 1752–1765). https://doi.org/10.1142/9789811275135_0160

Cahoon, D. R. (2006). A review of major storm impacts on coastal wetland elevations. *Estuaries and Coasts*, *29*(6), 889–898. https://doi.org/10.1007/bf02798648

Cahoon, D. R., Reed, D. J., Day, J. W., Jr., Steyer, G. D., Boumans, R. M., Lynch, J. C., et al. (1995). The influence of Hurricane Andrew on sediment distribution in Louisiana coastal marshes. *Journal of Coastal Research*, 280–294.

Cao, Y., Li, C., & Dong, C. (2020). Atmospheric cold front-generated waves in the coastal Louisiana. *Journal of Marine Science and Engineering*, *8*(11), 900. https://doi.org/10.3390/jmse8110900

Carniello, L., Defina, A., Fagherazzi, S., & D'Alpaos, L. (2005). A combined wind wave–tidal model for the Venice lagoon, Italy. *Journal of Geophysical Research*, *110*(F4), F04007. https://doi.org/10.1029/2004jf000232

Castagno, K. A., Jiménez-Robles, A. M., Donnelly, J. P., Wiberg, P. L., Fenster, M. S., & Fagherazzi, S. (2018). Intense storms increase the stability of tidal bays. *Geophysical Research Letters*, *45*(11), 5491–5500. https://doi.org/10.1029/2018GL078208

Chen, B., Kou, Y., Wang, Y., Zhao, D., Liu, S., Liu, G., et al. (2021). Analysis of storm surge characteristics based on stochastic process. *AIMS Mathematics*, *6*(2), 1177–1190. https://doi.org/10.3934/math.2021072

Chmura, G. L., Anisfeld, S. C., Cahoon, D. R., & Lynch, J. C. (2003). Global carbon sequestration in tidal, saline wetland soils. *Global Biogeochemical Cycles*, *17*(4). https://doi.org/10.1029/2002gb001917

Christensen, A. L., Mallard, J. M., Nghiem, J., Simard, M., Pavelsky, T. M., & Lamb, M. P. (2022). Delta-X: Acoustic doppler current profiler channel surveys, MRD, Louisiana, 2021, V2 [Dataset]. ORNL DAAC. https://doi.org/10.3334/ORNLDAAC/2081

Church, J. A., & White, N. J. (2006). A 20th century acceleration in global sea-level rise. *Geophysical Research Letters*, *33*(1), L01602. https://doi.org/10.1029/2005gl024826

Cortese, L., & Fagherazzi, S. (2022). Fetch and distance from the bay control accretion and erosion patterns in Terrebonne marshes (Louisiana, USA). *Earth Surface Processes and Landforms*, *47*(6), 1455–1465. https://doi.org/10.1002/esp.5327

Cortese, L., & Fagherazzi, S. (2023). Delta-X: Delft3D broad-scale sediment model, Terrebonne Basin, MRD, Louisiana, USA [Dataset]. ORNL DAAC, Oak Ridge, Tennessee, USA. https://doi.org/10.3334/ORNLDAAC/2301

Costanza, R., d'Arge, R., De Groot, R., Farber, S., Grasso, M., Hannon, B., et al. (1997). The value of the world's ecosystem services and natural capital. *Nature*, *387*(6630), 253–260. https://doi.org/10.1038/387253a0

Couvillion, B. R., Beck, H., Schoolmaster, D., & Fischer, M. (2017). Land area change in coastal Louisiana (1932 to 2016). In *USGS Scientific Investigations Map 3381*. U.S. Geological Survey. Retrieved from https://pubs.usgs.gov/sim/3381/sim3381_pamphlet.pdf

Cunge, J. A. (2003). Of data and models. *Journal of Hydroinformatics*, *5*(2), 75–98. https://doi.org/10.2166/hydro.2003.0007

Day, J. W., Jr., & Templet, P. H. (1989). Consequences of sea level rise: Implications from the Mississippi Delta. *Coastal Management*, *17*(3), 241–257. https://doi.org/10.1080/08920758909362088

De Vet, P. L. M., van Prooijen, B. C., Colosimo, I., Steiner, N., Ysebaert, T., Herman, P. M. J., & Wang, Z. B. (2020). Variations in storm-induced bed level dynamics across intertidal flats. *Scientific Reports*, *10*(1), 1–15. https://doi.org/10.1038/s41598-020-69444-7

Dingler, J. R., & Reiss, T. E. (1990). Cold-front driven storm erosion and overwash in the central part of the Isles Dernieres, a Louisiana barrier-island arc. *Marine Geology*, *91*(3), 195–206. https://doi.org/10.1016/0025-3227(90)90036-j

Everett, T., Chen, Q., Karimpour, A., & Twilley, R. (2019). Quantification of swell energy and its impact on wetlands in a deltaic estuary. *Estuaries and Coasts*, *42*(1), 68–84. https://doi.org/10.1007/s12237-018-0454-z

Ewald, M. J. (2013). Where's the ground surface? Elevation bias in LIDAR-derived digital elevation models due to dense vegetation in Oregon tidal marshes.

Fagherazzi, S. (2014). Storm-proofing with marshes. *Nature Geoscience*, *7*(10), 701–702. https://doi.org/10.1038/ngeo2262

Fagherazzi, S., Carniello, L., D'Alpaos, L., & Defina, A. (2006). Critical bifurcation of shallow microtidal landforms in tidal flats and salt marshes. *Proceedings of the National Academy of Sciences of the United States of America*, *103*(22), 8337–8341. https://doi.org/10.1073/pnas.0508379103

Fagherazzi, S., Mariotti, G., Leonardi, N., Canestrelli, A., Nardin, W., & Kearney, W. S. (2020). Salt marsh dynamics in a period of accelerated sea level rise. *Journal of Geophysical Research: Earth Surface*, *125*(8), e2019JF005200. https://doi.org/10.1029/2019JF005200

Fagherazzi, S., & Priestas, A. M. (2010). Sediments and water fluxes in a muddy coastline: Interplay between waves and tidal channel hydrodynamics. *Earth Surface Processes and Landforms: The Journal of the British Geomorphological Research Group*, *35*(3), 284–293. https://doi.org/10.1002/esp.1909

Fagherazzi, S., & Wiberg, P. L. (2009). Importance of wind conditions, fetch, and water levels on wave-generated shear stresses in shallow intertidal basins. *Journal of Geophysical Research*, *114*(F3), F03022. https://doi.org/10.1029/2008jf001139

Feng, Z., & Li, C. (2010). Cold-front-induced flushing of the Louisiana Bays. *Journal of Marine Systems*, *82*(4), 252–264. https://doi.org/10.1016/j.jmarsys.2010.05.015

Folse, T. M., Sharp, L. A., West, J. L., Hymel, M. K., Troutman, J. P., McGinnis, T. E., et al. (2018). *A standard operating procedures manual for the Coastwide reference monitoring system-wetlands: Methods for site establishment, data collection, and quality assurance/quality control* (p. 226). Louisiana Coastal Protection and Restoration Authority. 2008.

Georgiou, I. Y., FitzGerald, D. M., & Stone, G. W. (2005). The impact of physical processes along the Louisiana coast. *Journal of Coastal Research*, 72–89. Retrieved from http://www.jstor.org/stable/25737050

Green, M. O., & Coco, G. (2014). Review of wave-driven sediment resuspension and transport in estuaries. *Reviews of Geophysics*, *52*(1), 77–117. https://doi.org/10.1002/2013rg000437

Guo, B., Subrahmanyam, M. V., & Li, C. (2020). Waves on Louisiana continental shelf influenced by atmospheric fronts. *Scientific Reports*, *10*(1), 272. https://doi.org/10.1038/s41598-019-55578-w

Hartley, S., Pace, R., III, Johnston, J. B., Swann, M., O'Neil, C., Handley, L., & Smith, L. (2000). *A GAP analysis of Louisiana: Final report and data*. U.S. Department of the Interior, U.S. Geological Survey.

Hiatt, M., Snedden, G., Day, J. W., Rohli, R. V., Nyman, J. A., Lane, R., & Sharp, L. A. (2019). Drivers and impacts of water level fluctuations in the Mississippi River delta: Implications for delta restoration. *Estuarine, Coastal and Shelf Science*, *224*, 117–137. https://doi.org/10.1016/j.ecss.2019.04.020

Holthuijsen, L. H., Booij, N., & Ris, R. (1993). A spectral wave model for the coastal zone. In *Ocean wave measurement and analysis* (pp. 630–641). American Society of Civil Engineers.

Hopkinson, C. S., Cai, W. J., & Hu, X. (2012). Carbon sequestration in wetland dominated coastal systems—A global sink of rapidly diminishing magnitude. *Current Opinion in Environmental Sustainability*, *4*(2), 186–194. https://doi.org/10.1016/j.cosust.2012.03.005

Hopkinson, C. S., Morris, J. T., Fagherazzi, S., Wollheim, W. M., & Raymond, P. A. (2018). Lateral marsh edge erosion as a source of sediments for vertical marsh accretion. *Journal of Geophysical Research: Biogeosciences*, *123*(8), 2444–2465. https://doi.org/10.1029/2017jg004358

Houttuijn Bloemendaal, L. J., FitzGerald, D. M., Hughes, Z. J., Novak, A. B., & Georgiou, I. Y. (2023). Reevaluating the wave power-salt marsh retreat relationship. *Scientific Reports*, *13*(1), 2884. https://doi.org/10.1038/s41598-023-30042-y

Howes, N. C., FitzGerald, D. M., Hughes, Z. J., Georgiou, I. Y., Kulp, M. A., Miner, M. D., et al. (2010). Hurricane-induced failure of low salinity wetlands. *Proceedings of the National Academy of Sciences of the United States of America*, *107*(32), 14014–14019. https://doi.org/10.1073/pnas.0914582107

Jankowski, K. L., Törnqvist, T. E., & Fernandes, A. M. (2017). Vulnerability of Louisiana's coastal wetlands to present-day rates of relative sea-level rise. *Nature Communications*, *8*(1), 14792. https://doi.org/10.1038/ncomms14792

Jensen, D. J., Cavanaugh, K. C., Thompson, D. R., Fagherazzi, S., Cortese, L., & Simard, M. (2022). Leveraging the historical Landsat catalog for a remote sensing model of wetland accretion in coastal Louisiana. *Journal of Geophysical Research: Biogeosciences*, *127*(6), e2022JG006794. https://doi.org/10.1029/2022jg006794

Karl, T. R., Melillo, J. M., & Peterson, T. C. (2009). *Global climate change impacts in the United States: A state of knowledge report from the US Global change research Program*. Cambridge University Press.

Knutson, T. R., McBride, J. L., Chan, J., Emanuel, K., Holland, G., Landsea, C., et al. (2010). Tropical cyclones and climate change. *Nature Geoscience*, *3*(3), 157–163. https://doi.org/10.1038/ngeo779

LBSE (Louisiana Board of State Engineers). (1904). Report of the board of state engineers of the state of Louisiana. In *The Advocate* (p. 235).

Leonardi, N., Carnacina, I., Donatelli, C., Ganju, N. K., Plater, A. J., Schuerch, M., & Temmerman, S. (2018). Dynamic interactions between coastal storms and salt marshes: A review. *Geomorphology*, *301*, 92–107. https://doi.org/10.1016/j.geomorph.2017.11.001

Leonardi, N., Defne, Z., Ganju, N. K., & Fagherazzi, S. (2016). Salt marsh erosion rates and boundary features in a shallow Bay. *Journal of Geophysical Research: Earth Surface*, *121*(10), 1861–1875. https://doi.org/10.1002/2016jf003975

Leonardi, N., & Fagherazzi, S. (2014). How waves shape salt marshes. *Geology*, *42*(10), 887–890. https://doi.org/10.1130/g35751.1

Leonardi, N., & Fagherazzi, S. (2015). Effect of local variability in erosional resistance on large-scale morphodynamic response of salt marshes to wind waves and extreme events. *Geophysical Research Letters*, *42*(14), 5872–5879. https://doi.org/10.1002/2015gl064730

Lesser, G. R., Roelvink, J. V., van Kester, J. T. M., & Stelling, G. S. (2004). Development and validation of a three-dimensional morphological model. *Coastal Engineering*, *51*(8–9), 883–915. https://doi.org/10.1016/j.coastaleng.2004.07.014

Liu, K., Chen, Q., Hu, K., Xu, K., & Twilley, R. R. (2018). Modeling hurricane-induced wetland-bay and bay-shelf sediment fluxes. *Coastal Engineering*, *135*, 77–90. https://doi.org/10.1016/j.coastaleng.2017.12.014

Love, M. R., Caldwell, R. J., Carignan, K. S., Eakins, B. W., & Taylor, L. A. (2010). Digital elevation models of southern Louisiana: Procedures [Dataset]. Data Sources and Analysis, *22*. Retrieved from https://www.ncei.noaa.gov/metadata/geoportal/rest/metadata/item/gov.noaa.ngdc.mgg.dem:1521/html

Luk, S. Y., Todd-Brown, K., Eagle, M., McNichol, A. P., Sanderman, J., Gosselin, K., & Spivak, A. C. (2021). Soil organic carbon development and turnover in natural and disturbed salt marsh environments. *Geophysical Research Letters*, *48*(2), e2020GL090287. https://doi.org/10.1029/2020gl090287

Ma, Z., Ysebaert, T., van der Wal, D., de Jong, D. J., Li, X., & Herman, P. M. (2014). Long-term salt marsh vertical accretion in a tidal bay with reduced sediment supply. *Estuarine, Coastal and Shelf Science*, *146*, 14–23. https://doi.org/10.1016/j.ecss.2014.05.001

Marani, M., D'Alpaos, A., Lanzoni, S., & Santalucia, M. (2011). Understanding and predicting wave erosion of marsh edges. *Geophysical Research Letters*, *38*(21), L21401. https://doi.org/10.1029/2011gl048995

Mariotti, G., & Carr, J. (2014). Dual role of salt marsh retreat: Long-term loss and short-term resilience. *Water Resources Research*, *50*(4), 2963–2974. https://doi.org/10.1002/2013WR014676

Mariotti, G., Fagherazzi, S., Wiberg, P. L., McGlathery, K. J., Carniello, L., & Defina, A. (2010). Influence of storm surges and sea level on shallow tidal basin erosive processes. *Journal of Geophysical Research*, *115*(C11), C11012. https://doi.org/10.1029/2009jc005892

Mariotti, G., Huang, H., Xue, Z., Li, B., Justic, D., & Zang, Z. (2018). Biased wind measurements in estuarine waters. *Journal of Geophysical Research: Oceans*, *123*(5), 3577–3587. https://doi.org/10.1029/2017JC013748

McLoughlin, S. M., Wiberg, P. L., Safak, I., & McGlathery, K. J. (2015). Rates and forcing of marsh edge erosion in a shallow coastal bay. *Estuaries and Coasts*, *38*(2), 620–638. https://doi.org/10.1007/s12237-014-9841-2

Mendelssohn, I. A., & Kuhn, N. L. (2003). Sediment subsidy: Effects on soil–plant responses in a rapidly submerging coastal salt marsh. *Ecological Engineering*, *21*(2–3), 115–128. https://doi.org/10.1016/j.ecoleng.2003.09.006

Mitchell, M., Herman, J., Bilkovic, D. M., & Hershner, C. (2017). Marsh persistence under sea-level rise is controlled by multiple, geologically variable stressors. *Ecosystem Health and Sustainability*, *3*(10), 1379888. https://doi.org/10.1080/20964129.2017.1396009

Moeller, C. C., Huh, O. K., Roberts, H. H., Gumley, L. E., & Menzel, W. P. (1993). Response of Louisiana coastal environments to a cold front passage. *Journal of Coastal Research*, 434–447. Retrieved from http://www.jstor.org/stable/4298101

Murray, S. P., Walker, N. D., & Adams, C. E. (1993). Impacts of winter storms on sediment transport within the Terrebonne Bay Marsh Complex. *Processes of Coastal Wetlands Loss in Louisiana*, 41.

Neubauer, S. C. (2008). Contributions of mineral and organic components to tidal freshwater marsh accretion. *Estuarine, Coastal and Shelf Science*, *78*(1), 78–88. https://doi.org/10.1016/j.ecss.2007.11.011

Nyman, J. A., Crozier, C. R., & DeLaune, R. D. (1995). Roles and patterns of hurricane sedimentation in an estuarine marsh landscape. *Estuarine, Coastal and Shelf Science*, *40*(6), 665–679. https://doi.org/10.1006/ecss.1995.0045

Pannozzo, N., Leonardi, N., Carnacina, I., & Smedley, R. (2021). Salt marsh resilience to sea-level rise and increased storm intensity. *Geomorphology*, *389*, 107825. https://doi.org/10.1016/j.geomorph.2021.107825

Pannozzo, N., Leonardi, N., Carnacina, I., & Smedley, R. K. (2023). Storm sediment contribution to salt marsh accretion and expansion. *Geomorphology*, *430*, 108670. https://doi.org/10.1016/j.geomorph.2023.108670

Parker, K. R. (2014). Field and numerical investigation of wave power and shoreline retreat in Terrebonne Bay, Southern Louisiana [Dataset]. Louisiana State University and Agricultural & Mechanical College. Retrieved from https://repository.lsu.edu/gradschool_theses/4125

Penland, S., Roberts, H. H., Williams, S. J., Sallenger, A. H., Jr., Cahoon, D. R., Davis, D. W., & Groat, C. G. (1990). Coastal land loss in Louisiana.

Perez, B. C., Day, J. W., Jr., Rouse, L. J., Shaw, R. F., & Wang, M. (2000). Influence of Atchafalaya River discharge and winter frontal passage on suspended sediment concentration and flux in Fourleague Bay, Louisiana. *Estuarine, Coastal and Shelf Science*, *50*(2), 271–290. https://doi.org/10.1006/ecss.1999.0564

Priestas, A. M., Mariotti, G., Leonardi, N., & Fagherazzi, S. (2015). Coupled wave energy and erosion dynamics along a salt marsh boundary, Hog Island Bay, Virginia, USA. *Journal of Marine Science and Engineering*, *3*(3), 1041–1065. https://doi.org/10.3390/jmse3031041

Reed, D. J. (1989). Patterns of sediment deposition in subsiding coastal salt marshes, Terrebonne Bay, Louisiana: The role of winter storms. *Estuaries*, *12*(4), 222–227. https://doi.org/10.2307/1351901

Reed, D. J., Spencer, T., Murray, A. L., French, J. R., & Leonard, L. (1999). Marsh surface sediment deposition and the role of tidal creeks: Implications for created and managed coastal marshes. *Journal of Coastal Conservation*, *5*(1), 81–90. https://doi.org/10.1007/bf02802742

Ris, R. C., Holthuijsen, L. H., & Booij, N. (1999). A third-generation wave model for coastal regions: 2. Verification. *Journal of Geophysical Research*, *104*(C4), 7667–7681. https://doi.org/10.1029/1998jc900123

Roberts, H. H., Huh, O. K., Hsu, S. A., Rouse, L. J., Jr., & Rickman, D. A. (1989). Winter storm impacts on the chenier plain coast of southwestern Louisiana.

Rodgers, J. C., Murrah, A. W., & Cooke, W. H. (2009). The impact of Hurricane Katrina on the coastal vegetation of the Weeks Bay Reserve, Alabama from NDVI data. *Estuaries and Coasts*, *32*(3), 496–507. https://doi.org/10.1007/s12237-009-9138-z

Rogers, J. N., Parrish, C. E., Ward, L. G., & Burdick, D. M. (2018). Improving salt marsh digital elevation model accuracy with full-waveform lidar and nonparametric predictive modeling. *Estuarine, Coastal and Shelf Science*, *202*, 193–211. https://doi.org/10.1016/j.ecss.2017.11.034

Sanks, K. M., Shaw, J. B., & Naithani, K. (2020). Field-based estimate of the sediment deficit in coastal Louisiana. *Journal of Geophysical Research: Earth Surface*, *125*(8), e2019JF005389. https://doi.org/10.1029/2019jf005389

Sasser, C. E., Visser, J. M., Mouton, E., Linscombe, J., & Hartley, S. B. (2014). Vegetation types in coastal Louisiana in 2013: U.S. In *Geological Survey Scientific Investigations Map 3290, 1 sheet, scale 1:550,000.* https://doi.org/10.3133/sim3290

Schuerch, M., Vafeidis, A., Slawig, T., & Temmerman, S. (2013). Modeling the influence of changing storm patterns on the ability of a salt marsh to keep pace with sea level rise. *Journal of Geophysical Research: Earth Surface*, *118*(1), 84–96. https://doi.org/10.1029/2012JF002471

Shaw, S. P., & Fredine, C. G. (1971). In *Wetlands of the United States: Their extent and their value to waterfowl and other wildlife* (Vol. 39). US Department of the Interior, Fish and Wildlife Service.

Smith, J. E., Bentley, S. J., Snedden, G. A., & White, C. (2015). What role do hurricanes play in sediment delivery to subsiding river deltas? *Scientific Reports*, *5*(1), 17582. https://doi.org/10.1038/srep17582

Smith, K. E., Terrano, J. F., Khan, N. S., Smith, C. G., & Pitchford, J. L. (2021). Lateral shoreline erosion and shore-proximal sediment deposition on a coastal marsh from seasonal, storm and decadal measurements. *Geomorphology*, *389*, 107829. https://doi.org/10.1016/j.geomorph.2021.107829

Sweet, W. V., Hamlington, B. D., Kopp, R. E., Weaver, C. P., Barnard, P. L., Bekaert, D., et al. (2022). *Global and regional sea level rise scenarios for the United States: Updated mean projections and extreme water level probabilities along U.S. Coastlines* NOAA Technical Report NOS 01 (p. 111). National Oceanic and Atmospheric Administration, National Ocean Service. Retrieved from https://oceanservice.noaa.gov/hazards/sealevelrise/noaa-nos-techrpt01-global-regional-SLR-scenarios-US.pdf

Syvitski, J. P., & Kettner, A. (2011). Sediment flux and the Anthropocene. *Philosophical Transactions of the Royal Society A: Mathematical, Physical & Engineering Sciences*, *369*(1938), 957–975. https://doi.org/10.1098/rsta.2010.0329

Syvitski, J. P., Kettner, A. J., Overeem, I., Hutton, E. W., Hannon, M. T., Brakenridge, G. R., et al. (2009). Sinking deltas due to human activities. *Nature Geoscience*, *2*(10), 681–686. https://doi.org/10.1038/ngeo629

Syvitski, J. P., Vorosmarty, C. J., Kettner, A. J., & Green, P. (2005). Impact of humans on the flux of terrestrial sediment to the global coastal ocean. *Science*, *308*(5720), 376–380. https://doi.org/10.1126/science.1109454

Temmerman, S., Govers, G., Wartel, S., & Meire, P. (2003). Spatial and temporal factors controlling short-term sedimentation in a salt and freshwater tidal marsh, Scheldt estuary, Belgium, SW Netherlands. *Earth Surface Processes and Landforms: The Journal of the British Geomorphological Research Group*, *28*(7), 739–755. https://doi.org/10.1002/esp.495

Tognin, D., D'Alpaos, A., Marani, M., & Carniello, L. (2021). Marsh resilience to sea-level rise reduced by storm-surge barriers in the Venice Lagoon. *Nature Geoscience*, *14*(12), 906–911. https://doi.org/10.1038/s41561-021-00853-7

Törnqvist, T. E., Jankowski, K. L., Li, Y. X., & González, J. L. (2020). Tipping points of Mississippi Delta marshes due to accelerated sea-level rise. *Science Advances*, *6*(21), eaaz5512. https://doi.org/10.1126/sciadv.aaz5512

Törnqvist, T. E., Paola, C., Parker, G., Liu, K. B., Mohrig, D., Holbrook, J. M., & Twilley, R. R. (2007). Comment on "wetland sedimentation from hurricanes Katrina and Rita". *Science*, *316*(5822), 201. https://doi.org/10.1126/science.1136780

Turner, R. E., Baustian, J. J., Swenson, E. M., & Spicer, J. S. (2006). Wetland sedimentation from hurricanes Katrina and Rita. *Science*, *314*(5798), 449–452. https://doi.org/10.1126/science.1129116

Turner, R. E., Swenson, E. M., Milan, C. S., & Lee, J. M. (2007). Hurricane signals in salt marsh sediments: Inorganic sources and soil volume. *Limnology & Oceanography*, *52*(3), 1231–1238. https://doi.org/10.4319/lo.2007.52.3.1231

Tweel, A. W., & Turner, R. E. (2012). Landscape-scale analysis of wetland sediment deposition from four tropical cyclone events. *PLoS One*, *7*(11), e50528. https://doi.org/10.1371/journal.pone.0050528

Tweel, A. W., & Turner, R. E. (2014). Contribution of tropical cyclones to the sediment budget for coastal wetlands in Louisiana, USA. *Landscape Ecology*, *29*(6), 1083–1094. https://doi.org/10.1007/s10980-014-0047-6

Twilley, R. R., Bentley, S. J., Chen, Q., Edmonds, D. A., Hagen, S. C., Lam, N. S.-N., et al. (2016). Co-evolution of wetland landscapes, flooding, and human settlement in the Mississippi River Delta Plain. *Sustainability Science*, *11*(4), 711–731. https://doi.org/10.1007/s11625-016-0374-4

Twilley, R. R., Day, J. W., Bevington, A. E., Castañeda-Moya, E., Christensen, A., Holm, G., et al. (2019). Ecogeomorphology of coastal deltaic floodplains and estuaries in an active delta: Insights from the Atchafalaya Coastal Basin. *Estuarine, Coastal and Shelf Science*, *227*, 106341. https://doi.org/10.1016/j.ecss.2019.106341

Valentine, K., & Mariotti, G. (2019). Wind-driven water level fluctuations drive marsh edge erosion variability in microtidal coastal bays. *Continental Shelf Research*, *176*, 76–89. https://doi.org/10.1016/j.csr.2019.03.002

Walters, D. C., & Kirwan, M. L. (2016). Optimal hurricane overwash thickness for maximizing marsh resilience to sea level rise. *Ecology and Evolution*, *6*(9), 2948–2956. https://doi.org/10.1002/ece3.2024

Wamsley, T. V., Cialone, M. A., Smith, J. M., Atkinson, J. H., & Rosati, J. D. (2010). The potential of wetlands in reducing storm surge. *Ocean Engineering*, *37*(1), 59–68. https://doi.org/10.1016/j.oceaneng.2009.07.018

Wang, F. C., Lu, T., & Sikora, W. B. (1993). Intertidal marsh suspended sediment transport processes, Terrebonne Bay, Louisiana, USA. *Journal of Coastal Research*, 209–220. Retrieved from http://www.jstor.org/stable/4298078

Wang, H., Piazza, S. C., Sharp, L. A., Stagg, C. L., Couvillion, B. R., Steyer, G. D., & McGinnis, T. E. (2017). Determining the spatial variability of wetland soil bulk density, organic matter, and the conversion factor between organic matter and organic carbon across coastal Louisiana, USA. *Journal of Coastal Research*, *33*(3), 507–517. https://doi.org/10.2112/jcoastres-d-16-00014.1

White, E., & Kaplan, D. (2017). Restore or retreat? Saltwater intrusion and water management in coastal wetlands. *Ecosystem Health and Sustainability*, *3*(1), e01258. https://doi.org/10.1002/ehs2.1258

Wiberg, P. L., Carr, J. A., Safak, I., & Anutaliya, A. (2015). Quantifying the distribution and influence of non-uniform bed properties in shallow coastal bays. *Limnology and Oceanography: Methods*, *13*(12), 746–762. https://doi.org/10.1002/lom3.10063

Wiberg, P. L., Fagherazzi, S., & Kirwan, M. L. (2020). Improving predictions of salt marsh evolution through better integration of data and models. *Annual Review of Marine Science*, *12*(1), 389–413. https://doi.org/10.1146/annurev-marine-010419-010610

Williams, S. J., Arsenault, M. A., Buczkowski, B. J., Reid, J. A., Flocks, J., Kulp, M. A., et al. (2006). Surficial sediment character of the Louisiana offshore continental shelf region: A GIS compilation (No. 2006-1195) [Dataset]. US Geological Survey. Retrieved from https://www.usgs.gov/programs/cmhrp/science/usseabed

Wilson, B. J., Servais, S., Charles, S. P., Davis, S. E., Gaiser, E. E., Kominoski, J. S., et al. (2018). Declines in plant productivity drive carbon loss from brackish coastal wetland mesocosms exposed to saltwater intrusion. *Estuaries and Coasts*, *41*(8), 2147–2158. https://doi.org/10.1007/s12237-018-0438-z

Wolman, M. G., & Miller, J. P. (1960). Magnitude and frequency of forces in geomorphic processes. *The Journal of Geology*, *68*(1), 54–74. https://doi.org/10.1086/626637

Wu, G., Shi, F., Kirby, J. T., Liang, B., & Shi, J. (2018). Modeling wave effects on storm surge and coastal inundation. *Coastal Engineering*, *140*, 371–382. https://doi.org/10.1016/j.coastaleng.2018.08.011

Yang, S. L., Friedrichs, C. T., Shi, Z., Ding, P. X., Zhu, J., & Zhao, Q. Y. (2003). Morphological response of tidal marshes, flats and channels of the outer Yangtze River mouth to a major storm. *Estuaries*, *26*(6), 1416–1425. https://doi.org/10.1007/BF02803650

Yu, S. Y., Törnqvist, T. E., & Hu, P. (2012). Quantifying Holocene lithospheric subsidence rates underneath the Mississippi Delta. *Earth and Planetary Science Letters*, *331*, 21–30. https://doi.org/10.1016/j.epsl.2012.02.021

Zhang, X., Jones, C. E., Oliver-Cabrera, T., Simard, M., & Fagherazzi, S. (2022). Using rapid repeat SAR interferometry to improve hydrodynamic models of flood propagation in coastal wetlands. *Advances in Water Resources*, *159*, 104088. https://doi.org/10.1016/j.advwatres.2021.104088

Zhong, H., Van Gelder, P. H. A. J. M., Van Overloop, P. J. A. T. M., & Wang, W. (2014). Application of a fast stochastic storm surge model on estimating the high water level frequency in the Lower Rhine Delta. *Natural Hazards*, *73*(2), 743–759. https://doi.org/10.1007/s11069-014-1104-9

Zhu, Q., & Wiberg, P. L. (2022). The importance of storm surge for sediment delivery to microtidal marshes. *Journal of Geophysical Research: Earth Surface*, *127*(9), e2022JF006612. https://doi.org/10.1029/2022jf006612